

Measurement of Star-Formation Rate from H α in field galaxies at z=1

Karl Glazebrook,¹ Chris Blake,² Frossie Economou,³ Simon Lilly,⁴ Matthew Colless⁵

¹ Anglo-Australian Observatory, PO Box 296, Epping, NSW 2121, AUSTRALIA

² Magdalen College, Oxford, OX1 4AU, UK

³ Joint Astronomy Centre, 660 North A'ohoku Place, University Park, Hilo, HI 96720, USA

⁴ Department of Astronomy, University of Toronto, 60 St George Street, Toronto, Ontario, M5S 3H8, Canada

⁵ Mt Stromlo and Siding Spring Observatories, Australian National University, Weston Creek, ACT 2611, Australia

arXiv:astro-ph/9808276v1 25 Aug 1998

25 February 2019

ABSTRACT

We report the results of *J*-band infrared spectroscopy of a sample of 13 $z = 1$ field galaxies drawn from the Canada-France Redshift Survey, targeting galaxies whose redshifts place the rest frame H α line emission from HII regions in between the bright night sky OH lines. As a result we detect emission down to a flux limit of $\simeq 10^{-16}$ ergs $\text{cm}^{-2} \text{s}^{-1}$ corresponding to a luminosity limit of $\simeq 10^{41}$ ergs at this redshift for a $H_0 = 50 \text{ km s}^{-1} \text{ Mpc}^{-1}$, $q_0 = 0.5$ cosmology. From these luminosities we derive estimates of the star-formation rates in these galaxies which are independent of previous estimates based upon their rest-frame ultraviolet (2800Å) luminosity. The mean star-formation rate at $z = 1$, from this sample, is found to be three times as high as the ultraviolet estimates. The dust extinction in these galaxies is inferred to be moderate, with a typical $A_V = 0.5\text{--}1.0$ mags, comparable to local field galaxies. This suggests that the bulk of star-formation is not heavily obscured.

Star-forming galaxies have the bluest colours and a preponderance of disturbed/interacting morphologies. We also investigate the effects of particular star-formation histories, in particular the role of bursts vs continuous star-formation in changing the detailed distribution of UV to H α emission. Generally we find that models dominated by short, overlapping, bursts at typically 0.2 Gyr intervals provide a better model for the data. The star-formation history of the Universe from Balmer lines is compiled and found to be 2–3 \times higher than that inferred from the UV *at all redshifts*. It can not yet be clearly established whether the star-formation rate falls off or remains constant at high-redshift.

Key words: surveys – cosmology: observations – galaxies: evolution – galaxies: star-burst – stars: formation

1 INTRODUCTION

The topic of the history of star-formation in the Universe has excited much interest in recent years, stimulated by the first observations of nearly-normal star-forming galaxies at $z > 3$ (Steidel *et al.* 1996). Previously high-redshift studies were limited to highly active galaxies that may be poor tracers of the typical star-formation history of the universe as a whole. Steidel *et al.* used the colour signature of the Lyman break/Lyman- α forest discontinuity being redshifted through optical filters to select high-redshift objects (Guhathakurta *et al.* 1990), these were subsequently confirmed spectroscopically on the 10m W.M. Keck telescope.

Comparison of these objects with the low-redshift ($z <$

1) samples of field galaxies (Lilly *et al.* 1995, Ellis *et al.*, 1996) appears to show a rise in the Universal star-formation rate from $z = 0$ to $z = 1$ and a drop-off at $z > 3$ indicating a star-formation peak in the $z = 1\text{--}2$ epoch (Madau *et al.* 1996). This is also inferred to be the epoch when large galaxies with classical elliptical and spiral morphologies are assembled: Hubble Space Telescope observations indicate they are extant at $z = 1$ (Brinchmann *et al.* 1998, Lilly *et al.* 1998) but absent in the $z > 3$ sample (Giavalisco *et al.* 1996, Lowenthal *et al.* 1997). Theoretical developments using galaxy formation simulations constrained by the observed evolution in the density of neutral gas from Lyman- α

QSO absorbers show qualitative agreement with this picture (Fall *et al.* 1996).

However these measurements of star-formation rate are based upon the measurement of ultraviolet continuum luminosity, 1500–2800Å in the rest-frame, assumed to be from young stellar populations. If dust extinction played a significant role in obscuring UV radiation they could be underestimated by large factors which may change the picture completely.

A more robust way to measure the star-formation rate of high-redshift galaxies would be to measure their luminosities in Balmer recombination lines. This radiation come from reprocessed ionising radiation emitted by young stars. This approach has two advantages: firstly the ionising radiation comes from more massive short lived stars than the softer 1500–2800Å UV and hence falls quickly to zero only 20 Myr after star-formation stops. Thus the Balmer luminosity is a more direct measure of the *instantaneous* star-formation rate. This contrasts with the UV which continues to rise as the stellar populations evolve, typically doubling for example between 10 and 1000 Myr at 1500Å. For H α the main dependence is directly on the Initial Mass Function and negligibly on the temporal evolution.

The second main advantage is that the Balmer radiation is emitted in the red part of the optical spectrum and is thus much less affected by any dust extinction or attenuation than the ultraviolet. For example for typical SMC and Milky Way extinction laws (Pei 1992) the 1500Å and 2800Å extinctions (in magnitudes) range from 2–7 times greater than that at H α (6563Å).

However to observe H α at high-redshift requires infrared spectroscopy, which has not been possible until recently because of the faintness of the sources involved. Pettini *et al.* (1998) have secured the first IR spectra of 5 of the $z > 3$ Steidel *et al.* galaxies, and obtained H β luminosities. In this paper we report the results of the first measurements of the H α line in a sample of normal $z \simeq 1$ field galaxies drawn from the Canada-France Redshift Survey (Lilly *et al.* 1995, Le Fevre *et al.* 1995, Lilly *et al.* 1995B, Hammer *et al.* 1995). This sample (hereafter ‘CFRS’) is a highly-complete redshift survey of a magnitude-selected ($I_{AB} < 22.5$) sample of normal field galaxies. The median redshift is 0.6, and galaxies extend out to $z = 1.3$. Because the sample is magnitude selected the $z \gtrsim 1$ end is dominated by luminous $L \sim L^*$ galaxies.

2 OBSERVATIONS AND DATA REDUCTION

The observations were carried out on May 10-11 and October 3-5 1996 at the UK Infrared Telescope in Hawaii using the CGS4 spectrograph (Wright 1994). We chose galaxies in the redshift range 0.790-1.048 so that the H α line would lie in the relatively clean part of the near-infrared *J*-band (1.17-1.34 μ m) where the atmospheric extinction is relatively low (< 15%). We also selected galaxies with detectable [OII] emission in the optical CFRS spectra which make up 85% of the CFRS sample at $z \sim 1$.

As well as absorption, the *J*-band is contaminated by numerous airglow OH emission lines, which increase the broad-band sky-brightness by a factor of 30 and hinders the detection of faint objects. Our observational strategy

was to observe at high-resolution with CGS4, thus resolving out the OH background. Because we already knew the galaxies’ redshifts from the optical spectra the limited wavelength coverage at high-resolution was not a problem. Moreover we could exclude galaxies whose redshifts would put the H α line on or close to an OH line. (A similar strategy was also adopted by Pettini *et al.*) We observed with the 150 lines/mm grating and the 1 arcsec/1 pixel slit giving a resolution $\lambda/\Delta\lambda = 2200$. We determined empirically that at this resolution OH lines contaminated 50% of the bandpass, *i.e.* we had to exclude 50% of the high-redshift galaxies, but in the remaining clean part of the bandpass the mean background was only 20% that of broad *J*.

Targets were acquired using the following procedure: first we ‘peaked-up’ on a very bright star ($V = 1 - 2$ mags) within 1–2 degrees of the target. This involves centering the star on the optical finder TV, reading the IR array in a continuous ‘MOVIE’ mode, and then adjusting the offset between the axis of CGS4 and the TV until the IR flux is maximised. This assures the IR slit is aligned with the TV crosshair. Then we went to a fainter star, typically 17th mag, within 1–2 arcmin of our target galaxy and measured off the same coordinate system, centered the star on the TV crosshair and did a blind offset on to the target galaxy. (The targets were too faint to see on the TV). We would then autoguide either on the offset star or another bright star in the region.

Observations were made stepping the InSb detector array in 0.5 pixel increments to fully sample the instrument profile and nodding the telescope ± 9 arcsec along the slit between ‘OBJECT’ and ‘SKY’ positions to facilitate sky-subtraction (though note the object is still on the slit in both positions). Individual exposures ranged from 10–15 minutes. The typical seeing was 1.0 arcsec. A total of 13 objects were observed: these are listed with their total exposure times in Table 1. Standard wavelength calibration and flatfield corrections were applied. The October observing run was affected by the spectrograph slit being jammed out of position which caused the lines to be tilted on the image. The shifts were measured by cross-correlation and the tilt corrected by re-interpolation.

Even with the resolved OH background accurate sky-subtraction is critical to detection of faint lines. To first order the sky can be removed by simply subtracting the pairs of offset frames, though this leaves residual signal due to temporal sky changes. To second order the residual sky was removed by performing a polynomial interpolation along the slit, excluding the two object regions, and subtracting. This leaves no systematic residual, though the regions near the OH lines are still noisier due to the extra Poisson contribution, with the result being a 2D image with a positive spectrum in the ‘OBJECT’ row and a negative spectrum in the ‘SKY’ row. For each image we also made a pixel mask to exclude bad pixels on the detector and regions with noisy OH residuals.

In many of the images there were strong H α and continuum detections. We summed all the H α lines with good detections, fitted Gaussians spectrally and spatially to define the typical line profile and then used this mean profile (with the pixel mask) to optimally extract all bright, faint and possibly non-detected objects in a consistent manner.

In most of our observations we found that the nega-

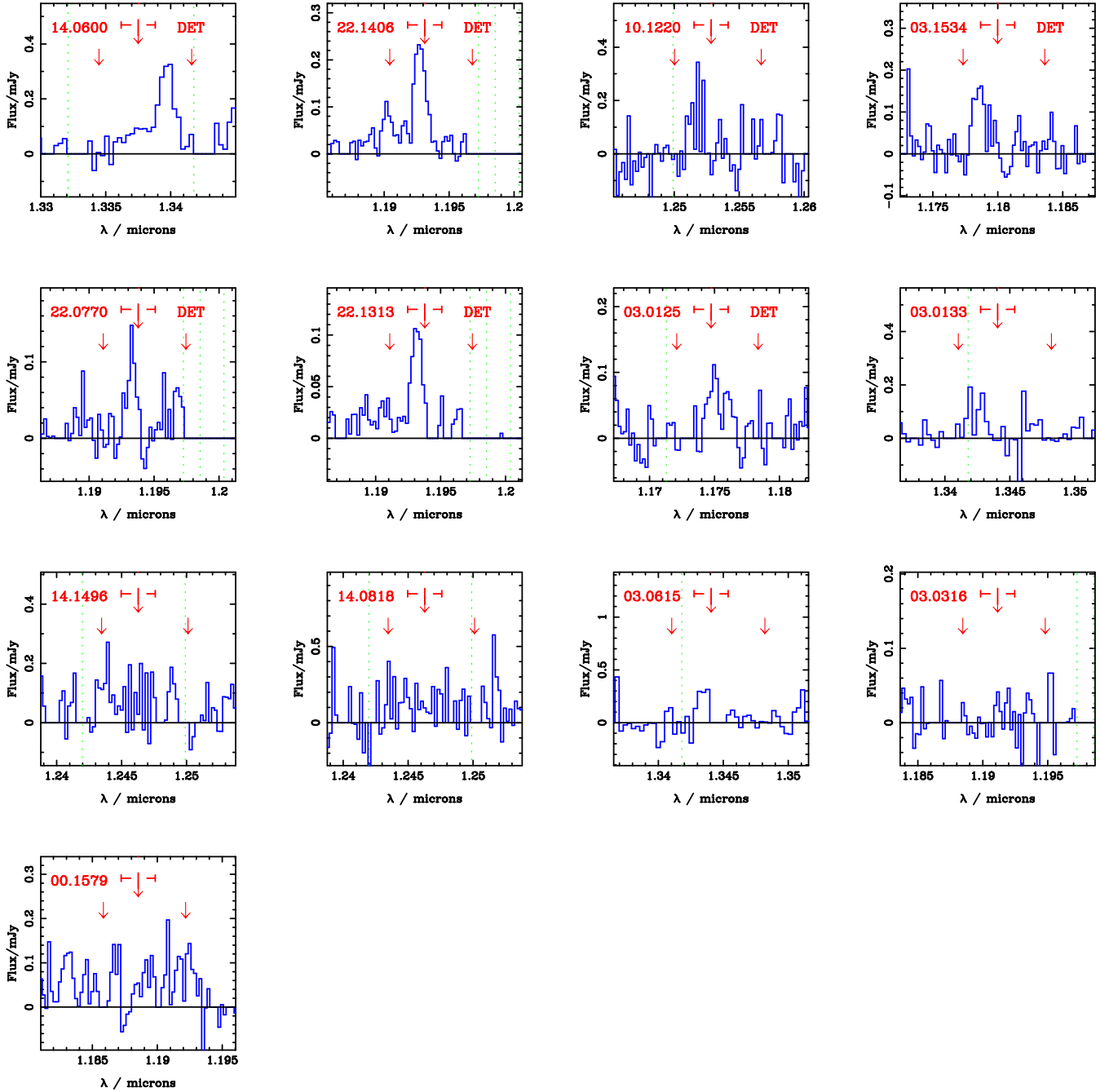


Figure 1. The J -band spectra of our CFRS galaxies. The spectra have been continuum subtracted and centered on the H α line. The large central arrow indicates the predicted H α position based on the optical redshift, the associated horizontal error bar denoting the 1σ error on the redshift. The two smaller arrows show the predicted positions of the [NII] 6548Å and 6583Å lines. The vertical dotted lines indicate the positions of strong night sky OH lines which have been masked out. The objects where we find a $> 2\sigma$ H α detection are labelled ‘DET.’

tive spectrum was typically weaker, or even absent, compared to the positive spectrum. This is attributed to the fact that any small errors in acquisition are magnified when stepping 9 arcsec away from the centre along the slit as the rotation is not precisely known. When there was a significant negative spectrum it was combined in a weighted manner (to maintain consistent exposure times) into the positive spectrum. This marginally increases the signal/noise,

though none of the flux measurements presented below are significantly changed if this step is omitted.

Next the spectra had atmospheric absorption removed using a smooth-spectrum standard and were flux calibrated using flux standards.

Finally we applied aperture corrections to allow for our finite 1.0 arcsec wide slit. Our objects are resolved, our mean Gaussian spatial profile along the slit of the H α line has a FWHM of 2.0 arcsec (which is consistent with the typical 3–

5 arcsec isophotal optical diameters measured for the CFRS sample (Hammer *et al.* 1997)). The flux calibration stars are observed through the same slit in 1.0 arcsec seeing. Assuming Gaussian profiles for both we derive a relative correction factor of 1.7, by which we multiply our spectra. While this can only be a rough correction, it gives fluxes consistent with the optical lines (see section 3). It is also only of order unity, so even if ignored our conclusions below are not drastically altered.

The continuum level was determined in each case by taking the mean of the data points ± 0.02 microns either side of the emission line, ignoring the masked points and the emission line, and was then subtracted from the data. The noise level of the data was determined empirically from the RMS in the same region. Next we computed the line flux by summing the flux $\pm N$ pixels around the line, excluding the masked pixels, where $N = 7$ is chosen to be the typical line FWHM. This is done regardless of whether there appears to be a detection or not (as the expected wavelength is known).

The final line fluxes and continuum fluxes (converted to AB mags and denoted J_C) are given in Table 1, along with the most useful CFRS parameters of our objects. $H\alpha$ fluxes $< 1\sigma$ are set = 0. We find 7 detections $> 2\sigma$ and 5 detections $> 3\sigma$ out of our 13 objects.

We convert these to luminosities using a $H_0 = 50$ km s $^{-1}$ Mpc $^{-1}$ and $q_0 = 0.5$ cosmology in Table 2. We use this cosmology for the rest of our paper. We note that in our further analysis our conclusions are based on comparing the luminosities of the same galaxies at different wavelengths, since all the galaxies in our sample lie close to $z = 1$ our conclusions are essentially unchanged if we use a different cosmology.

3 COMPLETENESS

In 10/13 of the spectra galaxy continuum emission was detected in addition to the $H\alpha$ emission line. This proves quite useful: we can check if our line non-detections are due to poor acquisition by comparing the continuum level of our line detections and non-detections. There is only one case in which there is no line *and* no continuum detection. The general trend is that the average continuum flux is *brighter* for the non-detections, this translates in to an median ($I - J_C$)_{AB} colour 0.7 mags *redder*. This argues against missing the object, in fact the trend towards redder colours is precisely what is expected for non-line emitting objects. We note that at $z = 1$ a E/S0 galaxy should have observed colours ($I - J$)_{AB} = 2.0 and a Scd galaxy ($I - J$)_{AB} = 1.0, using template SEDs from Kennicutt (1992). This is in line with the trend observed. Exact agreement is not expected as colours derived from long-slit spectra can only be very approximate due to refraction and aperture effects.

Figure 1 shows the final set of spectra, which have been continuum subtracted and centered on the $H\alpha$ line. The line is in all cases found within the error box given by the optical redshift ($\Delta z \simeq 0.002$). Our resolution is high enough that $H\alpha$ is well separated from the [NII] lines so we do not have to correct for blending. Also in a few cases (e.g. objects 22.1406 and 22.070) we see evidence for one of the weaker [NII] lines as well as the main $H\alpha$ line. This is additional evidence for the robustness of our detections. Note in many cases the

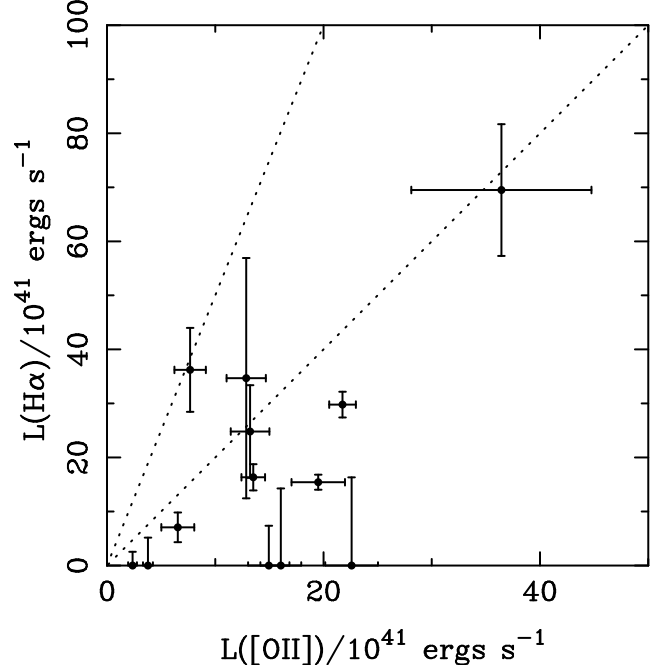


Figure 2. Comparison of line luminosities of the sample in [OII] and $H\alpha$. Dotted lines show slopes of $H\alpha/[OII] = 2$ and $H\alpha/[OII] = 5$

position of one or both of the [NII] lines is occluded by a noisy OH residual.

We can also test our completeness using CFRS values for the [OII] flux (Hammer *et al.* 1997) to calculate a [OII]/ $H\alpha$ line ratio. In the CFRS sample in this redshift range 85% of galaxies have [OII] emission. Hammer *et al.* tabulate the [OII] equivalent width and flux, the latter is aperture-corrected by comparing the spectra at $\sim 5500\text{\AA}$ with their V -band image photometry. Other than excluding galaxies with zero [OII] emission we made no attempt to concentrate on objects with the strongest [OII] emission. Thus the mean [OII] equivalent width (32 \AA) and range (10–60 \AA) of our small sub-sample are consistent with random sampling from the larger sample. The CFRS galaxies at $z = 1$ with zero [OII] are all at the red end of the colour distributions in $V - I$ and $I - K$. Thus the colours also indicate they are not significant star-forming systems and we conclude their exclusion has no significant impact on our conclusions below.

One might also ask the question: is the lack of $H\alpha$ detection in some of our objects consistent with the *presence* of [OII] in our optical spectra? This is addressed in Figure 2 where we plot the strength of the two lines against each other. It can be seen that given the $H\alpha$ error bars all points are consistent with a reasonable linear correlation. Kennicutt (1992) estimates the line ratio $H\alpha/[OII]$ from a range of local galaxies. He finds ratios of between 5 and 2 for normal spirals (1.0 mag mean extinction) and metal-poor low-extinction star-forming galaxies respectively. Our values tend to favour the lower $H\alpha/[OII]$ rather than the higher, i.e. a low extinction if interpreted as dust. This is consistent with our findings in Section 5. The points with zero $H\alpha$ are consistent with detected [OII] given the larger error bars. Note the line ratios are also good evidence that our aper-

ture corrections are reasonable, if omitted we would obtain a much lower ratio H α /[OII] = 1.

4 STAR FORMATION RATES FROM H α AND UV

Using models of population synthesis it is possible to calculate the relation between input star-formation rates and output UV and H α fluxes. The basic principle is that the UV light is dominated by short-lived main sequence stars (the H α light is reprocessed ionising UV) so the number of them in a galaxy is proportional to the star-formation rate. The prescription for this calculation is simple. For reference we outline it (and the corresponding assumptions) in detail:

(i) For a given time-dependent star-formation rate the population synthesis code gives the UV stellar spectrum as a function of time. Note that Kennicutt (1983) in deriving his calibration uses a simple grid of stars of different masses with evolutionary tracks current at the time.

(ii) For the UV continuum estimators one takes an averaged flux (e.g. through a synthetic box filter) at a specific wavelength (e.g. 1500 \AA , 2800 \AA). At the longer wavelengths, with increasing stellar lifetimes, the conversion from a constant star-formation rate to a UV flux is age-dependent (see for example Pettini *et al.* who uses different factors at 1500 \AA for 10^7 and 10^9 years). One then also needs to apply corrections for dust attenuation and/or Lyman absorption by line of sight systems (e.g. Madau 1995).

(iii) For H α one calculates the number of ionising Lyman continuum photons. This flux comes from the most short lived stars radiating at $\lambda < 912\text{\AA}$ with lifetimes of $\lesssim 10$ Myr. Then it is assumed all this radiation is absorbed by intervening hydrogen gas in the galaxy in which the forming stars are embedded and that none leaks out. In practice it seems this is very close to the truth. At very high-redshift the Lyman limit can be observed in the optical (e.g. the Steidel *et al.* galaxies) and the flux does indeed go to zero, but as these galaxies are identified by the Lyman breaks this could be a selection effect. For local galaxies there have been limited $\lambda < 912\text{\AA}$ spectroscopy, for example Leitherer *et al.* (1995) observed a sample of 4 starburst galaxies with the Hopkins Ultraviolet Telescope and concluded that $< 3\%$ of the ionising photons escaped. Constrained models of the ionising radiation field of the Milky Way (Bland-Hawthorn & Maloney 1997, 1998) indicate that approximately 5% may escape.

(iv) The ionising photons are reprocessed into recombination lines, and the relative strengths can be calculated in detail. Hummer & Storey (1987) calculate 0.45 H α photons are emitted per Lyman continuum photon for case B recombination. This number is quite robust, over a range of nebulosity conditions (10^2 – 10^6 K, 10^2 – 10^4 electrons cm^{-3}).

As there are a number of values for these conversion factors in the literature we thought it would be useful for reference purposes to systematically tabulate these for a set of models. This also serves to illustrate the range of variations and trends. The results of our calculations are given in Table 3 for UV 1500 \AA , 2800 \AA and H α conversions. The Bruzual & Charlot (1993, 1996) models ('BC96') offer a range of metallicities (albeit using theoretical model atmospheres —

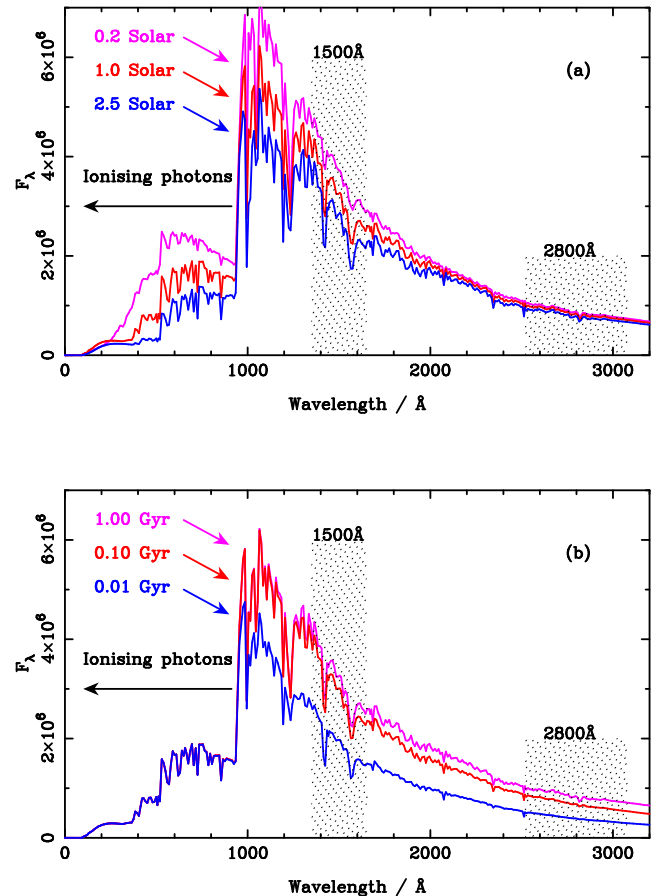


Figure 3. Illustration of the dependence of the UV spectrum on metallicity and time for a constant star-formation rate. These are theoretical galaxy spectra from the BC96 population synthesis models (Salpeter IMF). The position of the 1500 \AA and 2800 \AA $\pm 10\%$ bands are marked along with the ionising photons which are reprocessed into H α . The vertical order of the labels is the same as the vertical order of the spectra. Panel (a) shows the spectrum at 1 Gyr for a decreasing metallicity sequence. Panel (b) shows the solar metallicity spectrum for an increasing time sequence. It is easily seen that while the redder UV bands are relatively insensitive to metallicity they are strongly time dependent until 1 Gyr old. The reverse is true for the ionising photons — the stellar spectra below 912 \AA are identical for times > 20 Myr at a given metallicity. Hence the resulting H α flux is mainly dependent on metallicity.

the 'kl96' models). The PEGASE models (Fioc *et al.* 1997) offer two sets of post-main sequence evolutionary tracks but only solar metallicity. Both sets of models offer several Stellar Initial Mass Functions (IMFs); we tabulate the results using the IMFs of Salpeter (1955) and Scalo (1986) because these bracket the upper and lower limits of the variation. We also tabulate some other values given previously in the literature.

For all these models H α reaches a constant asymptote after 20 Myr, then stays constant to within a 5–10% out to 10 Gyr. Thus it can be used as a tracer of the instantaneous star-formation rate on time-scales of order ~ 10 Myr. For reference we give the value at 100 Myr. The conversion is very sensitive to the IMF, as the ionising flux comes from the most massive stars, with Salpeter giving a value 2.8 – $3.4 \times$

higher than Scalo for the different models. Another important point, which has not been remarked upon in the literature, is the strong effect of metallicity — the $\lambda < 912\text{\AA}$ EUV band contains numerous metal lines affecting the opacity of stellar atmospheres (the source of the ionising photons). At low metallicity the $\text{H}\alpha$ flux is about $1.7 \times$ that at solar metallicity for a given star-formation rate.

The average UV luminosity per unit Hz is computed as the total energy integrated through a $\pm 10\%$ box filter divided by the total bandwidth. This gives a negligible colour term. For a 10% filter the difference in the average between a constant f_ν spectrum (which approximates these spectra for $> 912\text{\AA}$) and a much redder constant f_λ spectrum is only 1%. The IMF dependence is somewhat less than for $\text{H}\alpha$ (typically a factor of 1.5–2.5) as these UV bands come from less massive stars and the metallicity dependence is much smaller as there is far less metal line absorption in this part of the continuum.

However there is a stronger time dependence, with the flux increasing significantly between 10^7 and 10^{10} years, especially at 2800\AA and for the Scalo IMF which is much less rich in massive stars. For cosmological times (> 1 Gyr) the 1500\AA flux is relatively insensitive to time as noted by Madau *et al.* (1998) (except for the extreme 0.02 Solar metallicity case). Thus it can be used as a tracer of the star-formation rate on time-scales of 1 Gyr. The 2800\AA flux is not as stable and changes at the 10–40% level over 1–10 Gyr. There are further $\lesssim 50\%$ variations in the exact conversion depending on the model and metallicity assumed.

These time and metallicity effects are illustrated graphically in Figure 3. Finally it is worth noting that the range in the *ratio* of $\text{H}\alpha$ to UV is less than the absolute range; as both come from high-mass stars the choice of IMF matters somewhat less.

5 THE STAR-FORMATION RATE AT $Z = 1$

Turning back to our data we can do a direct galaxy by galaxy comparison of the star-formation rates inferred from UV and $\text{H}\alpha$.

Our UV fluxes are particularly robust because for redshifts near unity the rest frame 2800\AA light corresponds very closely to the observed frame V -band light. To a first approximation we can simply ignore the K-correction and derive the 2800\AA flux directly from the CFRS V -magnitudes. We refine this slightly by using the SED fits from Lilly *et al.* (1996); this corrects the fluxes by 10–20%. Thus the UV luminosities we use are the same as the raw data which goes into the $z = 1$ star-formation rate determinations of Madau *et al.* (for $0.2 \leq z \leq 1$ this was based on the CFRS luminosity density functions of Lilly *et al.* 1996) We use a formal error bar of 20% for our UV fluxes to give errors representative of the V photometric errors and the K-corrections.

We plot the $\text{H}\alpha$ vs UV luminosities in Figure 4 and overlay lines for a set of conversions from Table 3. Note these are only valid for a continuous, constant star-formation rate — the more complex problem of bursts is considered below in Section 6.

It is clear from the plot that there is a order-of-magnitude agreement in the star-formation rates derived from the two methods and a reasonable correlation, i.e.

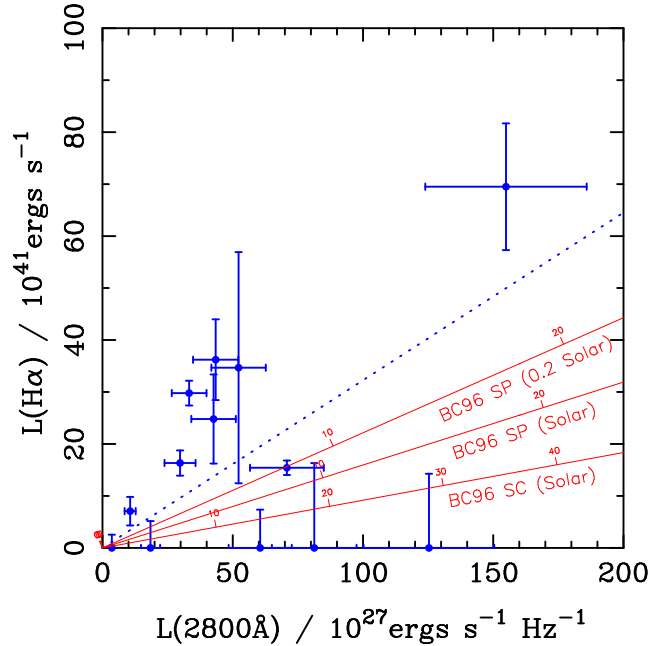


Figure 4. Comparison of the $\text{H}\alpha$ vs UV continuum flux at 2800\AA for the individual galaxies. The overlaid axes show the locus of constant star-formation rate for a set of fiducial models covering the range of UV/ $\text{H}\alpha$ ratios given in the last column of Table 3. The numeric labels on the axes are the corresponding star-formation rates in $M_\odot \text{yr}^{-1}$. The dotted line shows the ratio of the mean luminosity densities derived in Section 5.

strong UV systems are usually strong $\text{H}\alpha$ systems. There are no galaxies with an extremely large excess of $\text{H}\alpha$ relative to UV, which would occur if the star-formation was highly obscured by dust.

We do find points with zero $\text{H}\alpha$ flux and appreciable UV flux, which we would expect to detect within the measurement errors if there was a linear correlation. This can not be due to dust as the latter can only enhance the UV/ $\text{H}\alpha$ ratio not diminish it. As noted in Section 3, these spectra are detected, they just do not contain significant $\text{H}\alpha$. One physical effect that will explain this is the relative lifetimes of stars contributing to the UV and $\text{H}\alpha$ as mentioned in Section 4. When one moves away from the simple scenario of constant star-formation rate the picture changes considerably. For example for a instantaneous starburst the $\text{H}\alpha$ flux will drop to effectively zero after 30 Myr while significant UV flux will persist up to 1000 Myr. This will produce low $\text{H}\alpha$ points such as are seen in our sample. *Weak* $\text{H}\alpha$ should be present in *all our galaxies* because they are known to have [OII] emission (see Section 3), however the UV/ $\text{H}\alpha$ ratio will scatter more widely and it is certainly possible for $\text{H}\alpha$ to be below our detection limit despite significant [OII] and UV emission. To quantify these effects requires us to develop a proper model for starburst activity in galaxies. We do this below in Section 6.

Nevertheless when one averages over many galaxies the effect of bursts should cancel out in the mean — the continuous star-formation conversions of Table 3 should be applicable for an *ensemble* of galaxies. (This approximation is tested below using the methods developed in Section 6 and is found to accurate to $\sim \pm 10\%$, even for this small sam-

ple.) It can be seen that the values scatter about a ratio of 2–3 times as much star-formation inferred from the $\text{H}\alpha$ as UV. This is balanced to some extent by the zero points. By summing over *all* the galaxies we find the following relation between the luminosity per unit volume in $\text{H}\alpha$ and UV:

$$\frac{L(2800\text{\AA})}{L(\text{H}\alpha)} = 3.1 \pm 0.4$$

in the units of Table 3. This ratio is plotted as the dotted line in Figure 4.

The ratio is somewhat lower than those predicted by the models which give values in the range 5–14 for 0.2–2.5 Solar metallicities. What can cause this discrepancy? It is too large to be encompassed by our range of metallicities; one can boost the $\text{H}\alpha/\text{UV}$ ratio if we assume a younger age than ~ 1 Gyr. However changing to 0.1 Gyr only increases the slope by $\sim 30\%$; we could achieve the observed slope if star-formation is only ~ 0.01 Gyr old in all the detected galaxies but this would be unlikely simply due to random sampling — the redshift range of the sample corresponds to a timespan of $\simeq 1$ Gyr at $z = 1$. The most likely explanation for the discrepancy is the presence of dust extinguishing the ultraviolet light. If we adopt fiducial model values of (10.9, 6.3) for (Scalo, Salpeter) for Solar metallicity, which agree well between PEGASE and BC96 models (kl96 tracks), the ratio of $\text{H}\alpha$ to UV inferred star-formation rates are (3.5, 2.0).

Using Pei (1992) extinction formulae we then derive a mean sample A_V of (1.0, 0.5) mags for the SMC law, (1.1, 0.6) for the Galactic law. Calzetti *et al.* (1994) and Calzetti (1997) have proposed a greyer law for heavily reddened starbursts ($A_V \simeq 2.2$ mags). This appears inapplicable in our case as the Calzetti prescription has the nebular emission much more highly reddened than the stellar continuum. In particular the $\text{H}\alpha$ line extinction is greater than the 2800Å stellar extinction so the effect is the opposite of that we require. If we ignore this differential effect we derive A_V extinctions of (1.7, 0.9) mags.

Our extinction values are entirely consistent with what is found from studying of star-formation from Balmer lines in local normal Sab galaxies. For example Kennicutt (1983) found $A_V = 1.0$ mags and a study of low redshift $z < 0.3$ CFRS galaxies using the $H\beta/\text{H}\alpha$ line ratios by Tresse and Maddox (1998) found the same value.

Adopting the Milky Way law we can now also correct for the moderate extinction at $\text{H}\alpha$ and derive total star-formation rates. Comparing with the UV-derived values we find upwards correction factors of (8.0, 3.1) for (Scalo, Salpeter) IMFs. These numbers are the same to within $\pm 10\%$ for the SMC extinction law; this is because they differ most strongly in the UV at $<< 2800\text{\AA}$ (e.g. at the 2175Å dust feature) and in the near-UV and optical they are very similar. For the Calzetti law these numbers become (13.4, 4.2).

Finally we conclude that the average star-formation rate, after dust correction, of the $z \sim 1$ CFRS galaxies is $\sim (100, 20) M_\odot \text{ yr}^{-1}$ for (Scalo, Salpeter) IMFs, comparable to local starbursts (e.g. Calzetti 1997) and much greater than the typical $4 M_\odot \text{ yr}^{-1}$ found for local normal spirals (Kennicutt 1983) and the Milky Way (Smith *et al.* 1978).

6 MODELING OF STARBURSTS

As noted earlier the interpretation of $\text{H}\alpha$ and UV luminosities as star-formation rates becomes more complicated if non-constant star-formation histories are assumed. For this reason we developed a mathematical frame-work for exploring this and to see how well we could reproduce the observational distribution.

6.1 Methods

The principles are based upon maximum likelihood and are a 2D generalisation of the methods developed in Abraham *et al.* 1998 for colour-colour fitting. For a given star-formation history we can run a spectral evolution code and calculate $\text{H}\alpha$ and UV luminosity as a function of time using the methods of Section 4. We evolve the models for 5 Gyr and sample at random times (we can do this because all the galaxies are at similar redshift) to create a 2D model distribution of light in the the $(\text{H}\alpha, \text{UV})$ plane. The code then computes the likelihood of drawing the observational data from the model:

$$\mathcal{L} = \prod_i \int_{-\infty}^{\infty} \int_{-\infty}^{\infty} \frac{P(h, u) \exp \left(-\frac{(h_i - h)^2}{2\Delta h_i^2} - \frac{(u_i - u)^2}{2\Delta u_i^2} \right) du dh}{2\pi\Delta h_i \Delta u_i}$$

where the observational $(\text{H}\alpha, \text{UV})$ points are (h_i, u_i) with errors $(\Delta h_i, \Delta u_i)$, and the model points have probability density $P(h, u)$.

The star-formation histories are parameterised and likelihood space is explored to find the maximum likelihood. We use an adaptive algorithm where a large parameter space is explored with a coarse parameter grid to locate the peak and the region around the peak is then examined with a finer grid to give confidence limits on the fitted parameters from $\Delta\mathcal{L}$.

Once we have the best fit parameters for a model, we can then create simulated observational datasets. This is done 1000 times, the maximum likelihood fit being recomputed each time, this allows us to normalise our relative likelihood into an absolute probability of the observed data given the model.

6.2 Star-formation histories explored

We parameterised the star-formation histories as continuous star-formation, with galaxy to galaxy scatter, plus a random distribution of bursts. Initially the total star-formation rate is kept constant and normalised to the values derived in Section 5. This is a good approximation as an ensemble of galaxies undergoing bursts will approximate continuous star-formation and results in one less free parameter. For our further analysis we confine ourselves to the BC96 models (Solar metallicity, ‘kl96’ atmospheres) and the Salpeter IMF (as the latter gives better results for fitting the star-formation histories, colours and mass/light ratios of galaxies, see for example Kennicutt (1983) Madau *et al.* 1998, Calzetti 1997, Lilly *et al.* 1996). We then adopt the mean extinction derived above, $A_V = 0.6$ mags, and fit to the corrected $\text{H}\alpha$ and UV luminosity diagram.

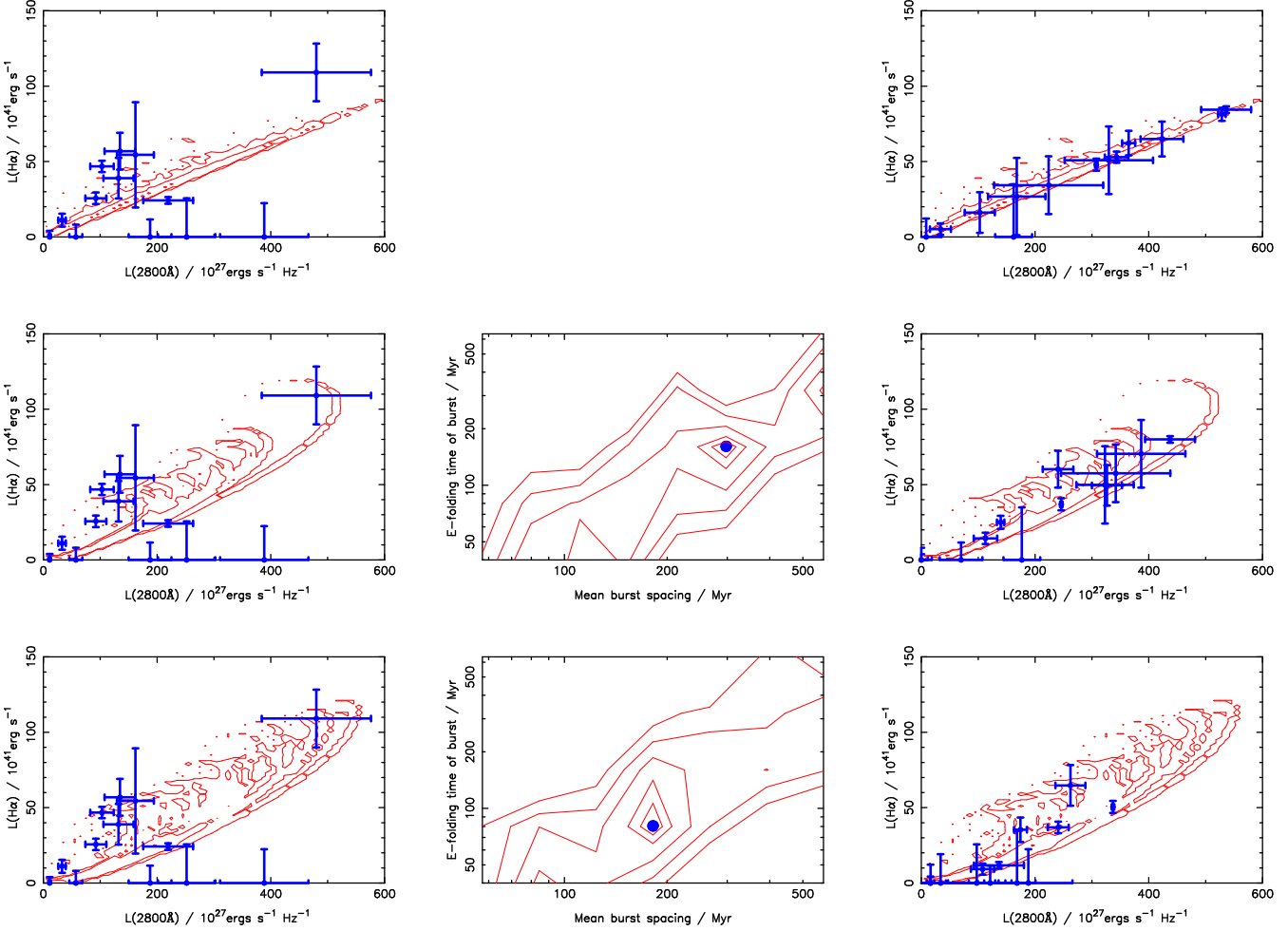


Figure 5. Results of fitting burst models to our extinction-corrected H α and UV (2800Å) data. The three rows show three different models as described in the text, they are: continuous star-formation (top row), fixed mass exponential bursts plus continuous star-formation (middle row) and variable mass exponential bursts plus continuous star-formation (bottom row). The left hand column of panels shows the observational data (points) compared with a model distribution generated from the best fit model (contours correspond to a factor of 10 in probability density). The middle column of panels show the likelihood contours of the main burst parameters generated by our fitting. (Contours correspond to a factor of 10 in likelihood, the circle marks the maximum likelihood point.) The right hand column show a *realisation* of the best fit model, *i.e.* 13 simulated data points generated from the model distribution with the observed errors (points $< 1\sigma$ are set = 0 as in the data). Note the continuous star-formation includes a component of galaxy-galaxy scatter.

To start with we modeled a simple continuous star-formation model to check our code was giving sensible results. To make it more realistic we introduced a scatter, C_σ , between galaxies following a normal distribution (slightly corrected to avoid negative star-formation rates).

The best fit results are shown in Figure 5 as a likelihood contour plot overlayed on the model points. For comparison we also show a simulated set of data points drawn from the model distribution. It can be seen that some scatter is introduced; this originates physically from the time variation of UV light even for constant star-formation. The best fit parameter values are shown in Table 4 — the model is a very bad fit to the distribution of data.

We next explored the effect of introducing starbursts on top of the continuous star-formation. Initially we tried fixed-mass bursts, then we tried a scheme for allowing the burst masses to vary. Since we could find little information in the literature as to an appropriate mass function

to adopt for bursts we invented our own simple phenomenological scheme: bursts are parameterised by a mean mass (M_μ) and standard deviation (M_σ). The distribution is assumed to be normal. While this has no physical basis it only has 2 parameters and at least allows us to investigate the effects of mass distributions. M_μ and our global star-formation rate normalisation fixes the mean interval between bursts. Finally we have F , the fraction of the star-formation occurring in bursts. For the form of the bursts we consider two cases (modeled after BC96): a constant burst of length τ and exponential bursts of e-folding time τ .

The results of this exercise is shown in Table 4. It can be seen that the burst models provide much better fits than the continuous models. The Monte-Carlo realisations show that the latter generate data sets like the observed one only about 1% of the time. This is because the continuous star-formation can not generate enough variation in the UV/H α ratio. The burst models are much better and generate syn-

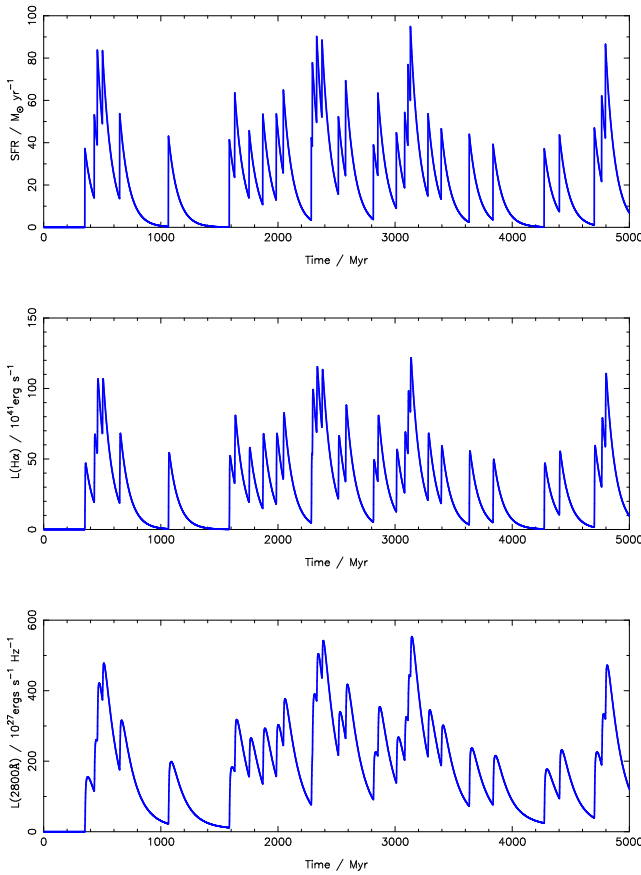


Figure 6. The star-formation rate, luminosity history in H α and UV (2800 \AA) typical of our best fit models. This is for the case of exponential bursts of variable mass, with a continuous star-formation component, *i.e.* the model shown in the lower 3 panels in Figure 5. It can be seen that for long inter-burst periods galaxies are indeed quiescent in H α , but not the UV.

thetic points which look like the data $\sim 10\text{--}20\%$ of the time. This is because the variation in the star-formation rate is the principle cause of variation in the UV/H α ratio. Allowing the burst mass to vary improves the fit only slightly, we conclude that our data does not constrain the shape of the burst mass function significantly. The best fit burst fraction is $\simeq 1$, indicating the burst mode is preferred. The results are illustrated graphically in the lower two rows of Figure 5 which compares the observational data with model realisations for a sample of key models. The likelihood contours of the main parameters are also shown.

The best fit mass of a typical burst is $2\text{--}5 \times 10^9 M_\odot$, corresponding to a time interval between bursts of typically $\sim 200\text{--}300$ Myr and the characteristic time τ is of $\sim 100\text{--}200$ Myr. This mean the bursts usually overlap in time. These values are similar to what one might expect intuitively based on the data: the chance of catching a galaxy in the H α quiescent stage has to be of order 1/3 to reproduce the fraction of points seen with UV but no H α .

We note that this kind of ‘continuous but episodic’ star-formation with several bursts per Gyr is of the same form as that found in local starburst galaxies by Calzetti (1997). Our average star-formation rates are of the same order too. In between bursts the star-formation rate and H α flux does

indeed drop close to zero while the UV persists (see Figure 6 which shows a sample time-dependence) due to the stellar lifetime effects mentioned in Section 4. Thus the zero H α points in our data (given the error bars) are naturally explained.

Finally with these tools we were able to test how well an ensemble of galaxies converged to approximating a continuous star-formation rate, as assumed in Section 5. To do this we re-ran the likelihood fitting, this time fitting for the total star-formation rate as a free parameter. The results of this gave rates of between 19 and 23 $M_\odot \text{ yr}^{-1}$ per galaxy, which agrees well with the value of $20 M_\odot \text{ yr}^{-1}$ calculated in Section 5 for the same Salpeter IMF.

While these simple models could do with some elaboration to obtain a better fit, we are near the limit of what can be inferred from 13 data points. It is clear this sort of detailed approach will benefit greatly from future observations and much larger samples.

7 MORPHOLOGICAL TRENDS

Six of the galaxies in our sample have morphological information from our programme of *Hubble Space Telescope* high-resolution imaging of CFRS and LDSS2 high-redshift galaxies (Brinchmann *et al.* 1998, Lilly *et al.*, 1998). This is obviously an even more limited sample, but we can look qualitatively at the dependence of star-formation rate on galaxy type.

The classifications are listed in Table 1 and postage stamps of the galaxies are shown in Figure 7. There are 3 galaxies classified as ‘Peculiar’. All have detected H α emission and blue colours ($(V - I)_{AB} < 1$) and one (14.0600) has the highest star-formation rate in our sample. Two of these are classed as ‘mergers’ and one as a close pair indicating an association between star-formation and interaction. There are two galaxies classed as ‘Compact’. Both of these are also blue ($(V - I)_{AB} < 1.2$) and it is interesting to note that while one has quiescent H α and strong UV the other has a large H α excess (3.2). Finally we have 03.0316 a red spiral ($(V - I)_{AB} = 2.9$) which is quiescent in both UV and H α .

Finally we note that galaxies with star-formation, whether inferred through H α or UV, have the bluest $V - I$ colours ($(V - I)_{AB} < 1.2$). This is not in contradiction with the modest extinction values derived in Section 5 — an extinction of $A_V = 0.6$ mags would only redden the observed $V - I$ (rest 2800 \AA – B) by a small 0.4 mags whereas the difference between and old and young stellar population is of order 2–3 mags.

8 COMPARISON WITH OTHER RESULTS

There are now enough measurements of Balmer line star-formation rates at high and low redshift to construct the first star-formation history of the Universe in Balmer light to compare with the previous UV measurements. For consistency we use the Salpeter IMF, $H_0 = 50 \text{ km s}^{-1} \text{ Mpc}^{-1}$, $q_0 = 0.5$ throughout. All points are re-derived from their original luminosity densities in a consistent manner using

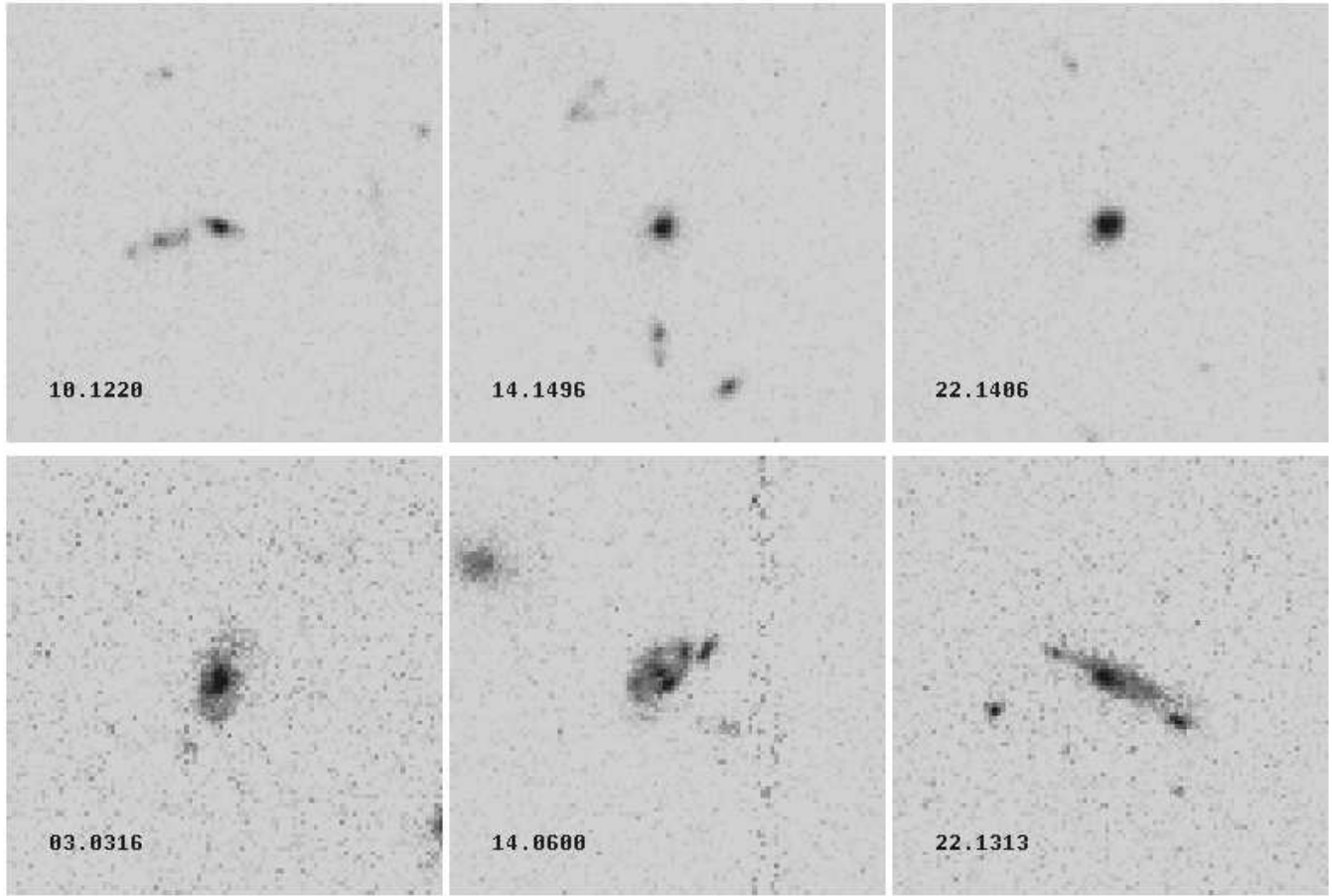


Figure 7. Postage stamps (10.1×10.1 arcsec) of the six galaxies having images from our HST morphology programme.

the UV, $H\alpha$ factors in Table 3 for BC96 (kl96) with Solar metallicity.

This is shown in Figure 8. The point at $z = 0$ comes from the Gallego *et al.* (1995) local objective prism survey and is based on $H\alpha$. Tresse and Maddox (1998) have measured the $H\alpha$ luminosity function at $z = 0.2$ from the CFRS, at which point $H\alpha$ is still available in the optical CFRS spectra. They find a value a factor of two higher than the UV measurements.

Our $H\alpha$ measurements are used to derive a new value for the star-formation rate density in the CFRS at $z = 1$. This is higher by a factor of $3.1 \times$ than the UV point. At $z > 3$ we show the points derived from the work of Pettini *et al.*, who used CGS4 to measure the $H\beta$ line in 5 of Steidel *et al.*'s galaxies. They infer star-formation rates 0.7-7 times higher than derived from the UV at 1500\AA rest and typical extinctions $A(1500\text{\AA}) = 1\text{--}2$ mags. We show this as a factor of 3 above the high-redshift UV points. As well as the Balmer lines we also plot the point of Hughes *et al.* based on sub-mm observations. This band measures UV reprocessed by dust as thermal radiation and hence is sensitive to galaxies which might not appear at all in the optical.

It can be seen that the general trend is for the Balmer line and sub-mm measurements to find values several times higher at all redshifts. The rise to $z = 1$ is preserved, ar-

guably the fall off at $z > 2$ is preserved though given the random errors and the systematics in the dust correction no change for $z > 1$ would also be consistent with the data. Whether star-formation peaks at intermediate redshift ($z = 1\text{--}2$) or continues to high redshifts ($z > 4$) is an important test of hierarchical formation scenarios (e.g. Baugh *et al.* 1998). From the current data the question must remain open.

An important point is that the dust corrections are not many times *larger*, then we have found. Larger corrections (e.g. $\times 15$) have been argued for by authors such as Meurer *et al.* (1997) based on amounts of obscuration in powerful starburst galaxies locally. However it is not clear that the local massive starburst galaxies (e.g. Arp 220) are the right analogs of the higher redshift field galaxies. When lower luminosity starburst galaxies are studied locally they prove much less obscured (e.g. Buat & Burgarella 1998), these systems are comparable in extinction to local spirals and the sample studied here.

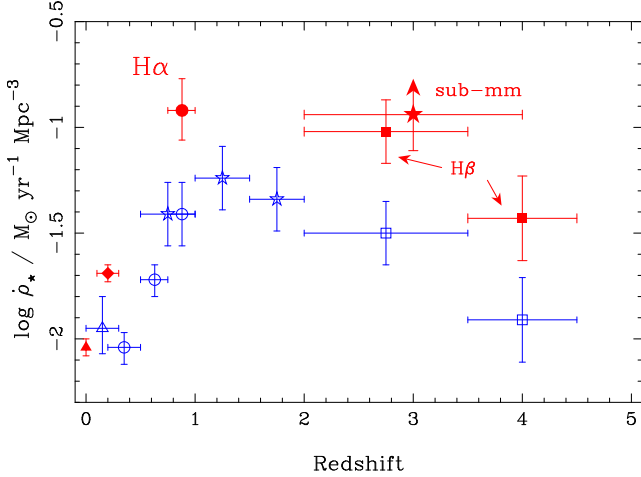


Figure 8. Star-formation history of the Universe inferred from Balmer lines (H α and H β) compared to UV determinations. The UV points are: Treyer *et al.* (1998; open triangle), Lilly *et al.* (1996; open circles), Connolly *et al.* (1997; open stars), Madau *et al.* (1996, 1998; open squares). The Balmer points are Gallego *et al.* (1995; filled triangle), Tresse & Maddox (1998; filled diamond), this work (filled circle), Pettini *et al.* (1998) correction of the UV Madau *et al.* points (filled squares). We also plot the sub-mm derived point of Hughes *et al.* 1998.

9 CONCLUSIONS

From a sample of 13 galaxies observed with CGS4 we have performed the first H α measurements of the star-formation rate at $z = 1$. We conclude the following:

- (i) The H α measurements show a star-formation rate approximately three as high as that inferred from the 2800Å continuum luminosity by Madau *et al.* (1996).
- (ii) The typical dust extinction is only moderate ($A_V = 0.5$ –1.0 mags) and very similar to that inferred in low redshift field galaxies.
- (iii) If there is a large population of obscured star-forming systems at $z = 1$ they are not common in known samples — there rate of occurrence in the CFRS at $z = 1$ must be $\lesssim 10\%$ or they would be detected in our data. This limit is similar to the results of Pettini *et al.* for the $z > 3$ Steidel *et al.* galaxies and consistent with deep sub-mm observations which estimate that massive obscured star-forming systems make up approximately 10% of high-redshift galaxies (Lilly *et al.* 1998b).
- (iv) The mean star-formation rate of a $z = 1$ CFRS galaxy is $\sim 20 M_\odot \text{ yr}^{-1}$ (for Salpeter IMF), which is enough to make such a L^* galaxy in a few Gyr. This is a factor of several higher than ordinary spiral galaxies of comparable luminosity today.
- (v) The large scatter in the distribution of H α to UV light is much better fit by a model in which star-formation occurs in episodic bursts with intervals of ~ 0.2 –0.3 Gyr and of length ~ 0.1 –0.2 Gyr. Pure continuous star-formation is strongly ruled out.
- (vi) We find qualitative trends for star-forming systems to have blue colours and peculiar morphology (especially interactions).
- (vii) The star-formation history of the Universe, as inferred from the Balmer lines, is qualitatively similar to that

inferred from the UV but corrected upwards by factors of approximately 2–3 at all redshifts. Although the overall form of a rise to $z = 1$ is preserved, a compilation of dust-insensitive data does not yet demonstrate with certainty whether there is a turnover beyond $z = 1$.

Finally, it is clear that the era of detailed spectral studies of high-redshift galaxies is upon us, made possible by the advent of intermediate to high-resolution spectrographs on 4m telescopes. In the next few years with larger samples and better near-IR spectrographs on 8m class telescopes (many with the ability to spatially resolve spectra in 2D) it will be possible to model the spectral evolution of the high-redshift galaxy population in much greater details. In particular the field will be able to focus much more on detailed astrophysics (stellar/dust/gas compositions, star-formation rates, dynamics, etc.) rather than simple statistics.

ACKNOWLEDGEMENTS

We are grateful to the UKIRT time assignment committee for their support of this programme and to the staff and telescope operators of the Joint Astronomy center for their support. We especially wish to thank Gillian Wright for technical and astronomical advice. The data reduction and analysis was performed primarily with computer hardware supplied by the Anglo-Australian Observatory and STARLINK. Special thanks go to Laurence Tresse and Francois Hammer of the CFRS team for making available there raw UV and [OII] data in machine-readable form. We would also like to thank Jarle Brinchmann and Richard Ellis for providing the HST images to allow us to explore the role of morphology. The interpretation of the data presented here was greatly aided by helpful discussions with many colleagues, especially Max Pettini, Joss Bland-Hawthorn, Carlos Frenk and Bob Abraham. We would also like to thank an anonymous questioner at the 1997 IAU meeting who prompted the authors into looking in to the detailed modeling of time-dependent H α and UV fluxes.

REFERENCES

Baugh C. M., Cole S., Frenk C. S., Lacey C. G., 1998, ApJ, 498, 504
 Bland-Hawthorn J., Maloney, P. R., 1997, PASA, 14, 59
 Bland-Hawthorn J., Maloney, P. R., 1998, ApJ, in press
 Brinchmann J., Abraham R., Schade D., Tresse L., Ellis R. S., Lilly S., Le Fevre O., Glazebrook K., Hammer F., Colless M. M., Crampton D., Broadhurst T., 1998, ApJ, 499, 112
 Buat V., Burgarella D., 1998, A&A, 334, 772
 Bruzual A. G., Charlot S., 1993, ApJ, 405, 538
 Bruzual A. G., Charlot S., 1996, documentation for BC96
 Calzetti D., Kinney A. L., Storchi-Bergmann T., 1994, ApJ, 429, 582
 Calzetti, D. 1997, AJ, 113, 162
 Connolly A. J., Szalay A. S., Dickinson M., Subbarao M. U., Brunner R. J., 1997, ApJ, 476, L11
 Ellis R. S., Colless M. M., Broadhurst T. J., Heyl J., Glazebrook K., 1996, MNRAS, 280, 235
 Fall S. M., Charlot S., Pei Y. C., 1996, ApJ, 464, L43
 Fioc M., Rocca-Volmerange B., 1997, A&A, 326, 950
 Gallego J., Zamorano J., Aragón-Salamanca A., Regg M., 1995, ApJ, 455, L1.

Giavalisco M., Steidel C. C., Macchetto F. D., 1996, *ApJ*, 470, 189

Guhathakurta P., Tyson J. A., Majewski S. R., 1990, *ApJ*, 357, 9

Hammer F., Crampton. D., Le Fevre O., Lilly S. J., 1995, *ApJ*, 455, 88

Hammer F., Flores H., Lilly S. J., Crampton D., Le Fevre O., Rola C., Mallen-Ornelas G., Schade D., Tresse L., 1997, *ApJ*, 481, 49

Hughes D., Serjeant S., Dunlop J., Rowan-Robinson M., Blain A., Mann R. G., Ivison R., Peacock J., Efstathiou A., Gear W., Oliver S., Lawrence A., Longair M., Goldschmidt P., Jenness T., 1998, *Nature*, 394, 241

Hummer D. G., Storey P. J., 1987, *MNRAS*, 224, 801

Kennicutt, R. C., 1983, *ApJ*, 272, 54

Kennicutt, R. C., 1992, *ApJ*, 388, 310

Leitherer C., Ferguson H. C., Heckman T. M., Lowenthal J. D., 1995, *ApJ*, 454, L19

Le Fevre O., Crampton. D., Lilly S. J., Hammer F., Tresse L., 1995, *ApJ*, 455, 60

Lilly S. J., Le Fevre O., Crampton. D., Hammer F., Tresse L., 1995, *ApJ*, 455, 50

Lilly S. J., Hammer F., Le Fevre O., Crampton. D., 1995B, *ApJ*, 455, 75

Lilly S. J., Le Fevre O., Hammer F., Crampton D., 1996, *ApJ*, 460, L1

Lilly S., Schade D., Ellis R., Le Fevre O., Brinchmann J., Tresse L., Abraham R., Hammer F., Crampton D., Colless M. M., Glazebrook K., Mallen-Ornelas G., Broadhurst T. J., 1998, *ApJ*, 500, 75

Lilly S. J., Eales S. A., Gear W. K., Bond J. R., Dunne L., Hammer F., Le Fevre O., Crampton D., 1998B, in *Proceedings of the 34th Liege International Astrophysics Colloquium "NGST: Science and Technological Challenges"*, (ESA), in press (astro-ph/9807261)

Lowenthal J. D., Koo D. C., Guzman R., Gallego J., Phillips A. C., Faber S. M., Vogt N. P., Illingworth G. D., Gronwall C., 1997, *ApJ*, 481, 673

Madau P., 1995, *ApJ*, 441, 18

Madau P., Ferguson H. C., Dickinson M. E., Giavalisco M., Steidel C. C., Fruchter A., 1996, *MNRAS*, 283, 1388

Madau P., Dickinson M. E., Pozzetti L., 1998, *ApJ*, 498, 106

Meurer G. R., Heckman T. M., Lehnert M. D., Leitherer C., Lowenthal J., 1997, *AJ*, 114, 54

Pei, Y. C. 1992, *ApJ*, 395, 130

Pettini M., Kellogg M., Steidel C. C., Dickinson M., Adelberger K. L., Giavalisco M., 1998, *ApJ*, in press (astro-ph/9806219)

Salpeter E. E., 1955, *ApJ*, 121, 161

Scalo J. M., 1986, *Fundam. Cosmic. Phys.*, 11, 1

Smith L. F., Biermann P., Mezger P. G., 1978, *Astr. Ap.*, 66, 65

Steidel C. C., Giavalisco M., Pettini M., Dickinson M., Adelberger K. L., 1996, *ApJ*, 462, L17

Tresse L., Maddox S. J., 1998, *ApJ*, 495, 691

Treyer M. A., Ellis R. S., Milliard B., Donas J., Bridges T. J., 1998, *MNRAS*, in press (astro-ph/9806056)

Wright G. S., 1994, *Experimental Astronomy*, 3, 17

Table 1.**OBSERVED SAMPLE AND FLUX MEASUREMENTS**

CFRS#	Exposure (secs)	z (mags)	I_{AB} (mags)	$(V - I)_{AB}$	EW [OII] (rest Å)	$F(\text{H}\alpha)$ $10^{-17} \text{ergs cm}^{-2} \text{s}^{-1}$	J_C (mags)	HST Morphology
00.1579	1000	0.811	22.40	1.45	33 ± 6	0.0 ± 13.9	18.87 ± 0.12	—
03.0125	1000	0.790	22.08	2.08	19 ± 7	20.1 ± 7.8	19.62 ± 0.17	—
03.0133	1500	1.048	22.45	1.00	65 ± 16	52.9 ± 33.9	19.89 ± 0.38	—
03.0316	1500	0.815	21.98	2.91	12 ± 2	0.0 ± 6.8	—	Spiral
03.0615	500	1.048	22.01	0.96	27 ± 5	0.0 ± 24.9	18.86 ± 0.25	—
03.1534	2000	0.798	22.45	0.70	39 ± 8	68.9 ± 23.8	—	—
10.1220	1200	0.909	22.36	0.97	20 ± 4	75.5 ± 16.2	—	Peculiar (merger)
14.0600	4000	1.038	21.53	0.69	27 ± 9	108.2 ± 19.0	18.76 ± 0.40	Peculiar (close pair)
14.0818	1000	0.899	21.02	1.12	19 ± 2	0.0 ± 30.5	19.10 ± 0.28	—
14.1496	2400	0.899	21.80	1.13	28 ± 6	0.0 ± 15.7	18.38 ± 0.13	Compact
22.0770	3000	0.819	21.78	1.58	39 ± 5	42.9 ± 6.4	19.23 ± 0.13	—
22.1313	6000	0.819	21.74	0.84	40 ± 5	40.5 ± 3.6	19.58 ± 0.12	Peculiar (merger)
22.1406	4000	0.818	22.16	1.16	55 ± 4	78.3 ± 6.2	18.62 ± 0.12	Compact

Table 2.**DERIVED LUMINOSITIES**

CFRS#	$L(\text{H}\alpha)$ $(10^{41} \text{ergs s}^{-1})$	$L(\text{[OII]})$ $(10^{41} \text{ergs s}^{-1})$	$L(2800\text{\AA})$ $(10^{27} \text{ergs s}^{-1} \text{Hz}^{-1})$
00.1579	0.0 ± 5.2	3.8 ± 0.5	18.5
03.0125	7.1 ± 2.8	6.5 ± 1.5	10.6
03.0133	34.7 ± 22.2	12.9 ± 1.8	52.2
03.0316	0.0 ± 2.5	2.4 ± 0.4	3.6
03.0615	0.0 ± 16.3	22.6 ± 2.4	81.3
03.1534	24.8 ± 8.6	13.2 ± 1.8	42.7
10.1220	36.2 ± 7.8	7.7 ± 1.4	43.5
14.0600	69.5 ± 12.2	36.4 ± 8.3	154.9
14.0818	0.0 ± 14.3	16.1 ± 1.9	125.3
14.1496	0.0 ± 7.4	14.9 ± 1.9	60.5
22.0770	16.3 ± 2.4	13.5 ± 1.1	29.8
22.1313	15.4 ± 1.4	19.5 ± 2.5	70.8
22.1406	29.8 ± 2.4	21.8 ± 1.2	33.3

Table 3.CONVERSIONS OF $H\alpha$,UV TO STAR-FORMATION RATESLuminosities are for $1 M_\odot \text{ yr}^{-1}$.

Model	Z/Z_\odot	IMF	$L(H\alpha)$ ($10^{41} \text{ ergs s}^{-1}$)	$L(1500\text{\AA})$ ($10^{27} \text{ ergs s}^{-1} \text{ Hz}^{-1}$)			$L(2800\text{\AA})$ ($10^{27} \text{ ergs s}^{-1} \text{ Hz}^{-1}$)			$\frac{L(2800\text{\AA})}{L(H\alpha)}$ (1 Gyr)
				0.1 Gyr	1.0 Gyr	3.0 Gyr	0.1 Gyr	1.0 Gyr	3.0 Gyr	
BC96 (kl96)	0.02	SC	0.68	4.36	6.64	7.19	2.84	6.23	8.63	9.2
BC96 (kl96)	0.20	SC	0.58	3.93	5.36	5.40	2.84	5.35	6.58	9.2
BC96 (kl96)	0.40	SC	0.50	3.80	4.82	4.83	2.89	4.96	5.80	9.9
BC96 (kl96)	1.00	SC	0.40	3.48	4.02	4.02	2.93	4.36	4.81	10.9
BC96 (kl96)	2.50	SC	0.28	3.07	3.33	3.33	2.93	3.88	4.10	13.9
BC96 (gs95)	1.00	SC	0.61	3.64	4.39	4.40	2.39	3.72	4.13	6.1
BC96 (gsHR)	1.00	SC	0.61	3.64	4.39	4.40	2.39	3.72	4.13	6.1
PEG (Pad)	1.00	SC	0.41	4.13	4.72	4.72	3.15	4.80	5.39	11.7
PEG (Gen)	1.00	SC	0.45	3.84	4.42	4.43	2.94	4.57	5.18	10.2
M98	1.00	SC			3.50			5.10		
BC96 (kl96)	0.02	SP	2.23	10.21	12.56	12.87	6.29	9.48	10.78	4.2
BC96 (kl96)	0.20	SP	1.96	9.27	10.93	10.96	6.32	8.85	9.53	4.5
BC96 (kl96)	0.40	SP	1.70	9.22	10.49	10.50	6.59	8.76	9.24	5.1
BC96 (kl96)	1.00	SP	1.35	8.61	9.37	9.37	6.85	8.46	8.73	6.3
BC96 (kl96)	2.50	SP	0.90	7.62	7.99	7.99	6.87	7.94	8.07	8.8
BC96 (gs95)	1.00	SP	1.97	8.73	9.77	9.77	5.50	7.00	7.25	3.6
BC96 (gsHR)	1.00	SP	1.97	8.73	9.77	9.77	5.50	7.00	7.25	3.6
PEG (Pad)	1.00	SP	1.19	8.64	9.31	9.31	6.16	7.68	7.97	6.5
PEG (Gen)	1.00	SP	1.28	8.02	8.66	8.66	5.68	7.16	7.46	5.6
K83	1.00	SP-like	1.12							
M96	1.00	SP			11.06			7.04		
M98	1.00	SP	1.41			8.00			7.90	

Notes:

- (i) SC and SP are the Scalo (1986) and Salpeter (1955) IMFs
- (ii) K83 is Kennicutt's (1983) conversion for a Salpeter-like IMF
- (iii) M96 is Madau *et al.* (1996) values for 0.1-1 Gyr, derived from Bruzual & Charlot (1993); M98 are the values from Madau *et al.* (1998)
- (iv) BC96 are values derived from Bruzual & Charlot (1996) models, multi-metallicity 'kl96' stellar spectra are based on stellar model atmospheres (Lejeune *et al.*, 1996, Kurucz, 1995) and 'gs95' are based on observed Gunn & Stryker (1983) spectra. All use the 'Padova' stellar evolutionary tracks.
- (v) PEG are values derived from the PEGASE models (Fioc *et al.* 1997) for the 'Padova' and 'Geneva' stellar evolutionary tracks respectively.

Table 4. Best fit model parameters

Description of model	Best fit parameters with errors, in the form $P_{\text{fitted}} = 2\sigma < 1\sigma < \text{best value} < 1\sigma < 2\sigma$	$\log(L_{\text{best}})$	Monte-Carlo deviation of L_{best} (percentiles)
Continuous star-formation rate	$C_\sigma = 0.61 < 0.65 < \mathbf{0.70} < - < -$	-38.42	98.6
Continuous plus constant starbursts of fixed mass	$F = 0.87 < 0.90 < \mathbf{1.00} < - < -$ C_σ not relevant because $F_{\text{best}} = 1.0$ $M_\mu = 1.23 < 1.31 < \mathbf{1.39} < 1.48 < 1.57 \times 10^9 M_\odot$ $\tau = - < 50.6 < \mathbf{80.0} < 88.4 < 97.8 \text{ Myr}$	-36.09	87.4
Continuous plus constant starbursts of variable mass	$F = 0.93 < 0.96 < \mathbf{1.00} < - < -$ C_σ not relevant because $F_{\text{best}} = 1.0$ $M_\mu = 1.57 < 1.84 < \mathbf{2.15} < 2.56 < 3.03 \times 10^9 M_\odot$ $M_\sigma = 0.18 < 0.22 < \mathbf{0.30} < 0.32 < 0.34$ $\tau = 65.9 < 72.6 < \mathbf{80.0} < 107.0 < 143.1 \text{ Myr}$	-35.88	82.0
Continuous plus exponential starbursts of fixed mass	$F = 0.83 < 0.94 < \mathbf{1.00} < - < -$ C_σ not relevant because $F_{\text{best}} = 1.0$ $M_\mu = 4.28 < 4.71 < \mathbf{5.18} < 5.54 < 5.93 \times 10^9 M_\odot$ $\tau = 122.7 < 140.1 < \mathbf{160.0} < 170.5 < 181.7 \text{ Myr}$	-36.21	88.4
Continuous plus exponential starbursts of variable mass	$F = 0.92 < 0.96 < \mathbf{1.00} < - < -$ C_σ not relevant because $F_{\text{best}} = 1.0$ $M_\mu = 2.67 < 2.91 < \mathbf{3.16} < 3.37 < 3.60 \times 10^9 M_\odot$ $M_\sigma = - < - < \mathbf{0.10} < 0.13 < 0.17$ $\tau = 65.0 < 72.1 < \mathbf{80.0} < 106.3 < 141.4 \text{ Myr}$	-36.04	88.0

Notes:

- (i) Parameter ranges ‘ 1σ ’ and ‘ 2σ ’ correspond to $\Delta \log \mathcal{L} = -0.5, -1.0$.
- (ii) M_σ is expressed as a fraction of M_μ .